Geotech Geol Eng (2017) 35:1169–1183
DOI 10.1007/s10706-017-0172-5

ORIGINAL PAPER

Empirical Formula of Shear Strength of Rock Fractures Based on 3D Morphology Parameters

Hangyu Dong · Baohua Guo · Yizhe Li · Kai Si · Long Wang

Received: 9 May 2016 / Accepted: 15 January 2017 / Published online: 23 January 2017
© Springer International Publishing Switzerland 2017

Abstract The prime objective of this work is to provide a reference to predict the peak shear strength of rock fractures. The paper studied some shear properties of rock fractures and proposed an empirical formula for the peak shear strength of rock fractures based on 3D morphology parameters. The rock fractures were induced in cylindrical sandstone and marble specimens by means of indirect tension. A rock direct shear apparatus (RDS-200) was adopted to conduct direct shear tests on five groups of rock fractures under different levels of normal load. Before the direct shear test, 3D morphology parameters of rock fracture surfaces were obtained using a 3D optical scanner. By analyses of direct shear test data, the relationships between peak shear strength, peak shear displacement, peak dilatancy angle, residual friction coefficient and peak normal stress were found. According to the evolution trends of peak shear strength and peak dilatancy angle along with the normal stress, an empirical formula was proposed to predict the peak shear strength of rock fractures in both sliding and cutting failure modes considering the 3D morphology parameters of rock fracture surfaces. The empirical formula could be commonly used for different types (sandstone and marble) and grain sizes (powder-grained, fine-grained, medium-grained and coarse-grained) of rock fractures.

Keywords Rock fracture · Direct shear test · 3D morphology parameter · Peak shear strength

H. Dong · B. Guo (✉) · Y. Li · K. Si · L. Wang
School of Energy Science and Engineering, Henan Polytechnic University, Jiaozuo 454000, People's Republic of China
e-mail: guobaohua@139.com

B. Guo
Collaborative Innovation Center of Coal Work Safety, Jiaozuo 454000, People's Republic of China

1 Introduction

Mechanical properties of rock fractures are relatively influenced by rock mechanical properties and 3D morphology parameters of rock fracture surfaces. Many geological discontinuities exist in natural rock mass, such as joints and faults, which greatly influence the rock mass stability. Engineering accidents caused by rock joints are common. Thus, it is important to be able to determine the strength and deformation properties of rock fractures. The determination of a general criterion to estimate the peak shear strength of rock fractures has been researched by many scholars for many years. Their research results are as follows.

Patton (1966) proposed a shear strength formula (1) for artificial joints based on the Coulomb friction law. It has been customary to fit Patton's linear relation:

$$\tau_p = \sigma_n \tan(\varphi_b + i_0) \quad (1)$$

where i_0 is the climbing slope angle, φ_b is the basic friction angle, τ_p is the peak shear strength, and σ_n is the normal stress.

The shear strength formula (2) proposed by Barton (1973) is as follow:

$$\tau_p = \sigma_n \tan\left[\varphi_b + JRC \log_{10}\left(\frac{JCS}{\sigma_n}\right)\right] \quad (2)$$

where *JRC* is joint roughness coefficient, *JCS* is joint compression strength and it can be estimated from Schmidt harmer tests. Basic friction angle (φ_b) was estimated from tilt tests on dry unweathered sawn rock surface. The joint roughness coefficient (*JRC*), joint compression strength (*JCS*) and normal stress (σ_n) are used to describe the climbing slope angle i_0 of rock joint surface. *JRC* value was estimated through tilt test or pull test by the following formula (Barton and Choubey 1977).

$$JRC = \frac{\alpha - \varphi_b}{\log_{10}(JCS/\sigma_{no})} \quad (3)$$

where α was the tilt angle when sliding occurs, σ_{no} was the corresponding value of effective normal stress when sliding occurs. As for field estimation of roughness, the a/L method (Barton and Bandis 1990) was prior to tilt test.

Except for *JRC*-*JCS* model, some models were also proposed to predict shear strength of rock joint. Ladanyi and Archambault (1970) developed a shear strength formula considering that shear resistance came from shear dilatancy, tooth-shaped inclined plane, normal stress and breaks of asperities, which was applied only to regular triangular joints. For irregular joints, Kusumi et al. (1997) proposed some experimental equations to represent the shear strength parameters included in Ladanyi's formula. Jing et al. (1993) proposed a 2D constitutive model of the rock joint, but the model could be applied to predict the shear behavior only when shear displacement was less than the largest size of asperities. Two failure mechanisms, in accordance with the normal load level, were proposed by Serrano et al. (2014), in which the first one appears for low normal stresses, whereas the second one occurs when normal stress is high. Indeed, among all the models proposed in the literature to estimate the shear strength of rock joints, Barton's criterion is the one that is mainly used in practice.

Methods aiming at calculating *JRC* value and checking on values of *JRC* estimated from tilt test, pull test or a/L method were proposed by many researchers (Tse and Cruden 1979; Lee et al. 1990; Sanei et al. 2015; Maerz et al. 1990; Xie et al. 1999). Statistical method and fractal method were also used to build the relationships between *JRC* and fractal dimension or statistics of joint profiles. Reeves (1985) gave the relationships among 3D morphology parameters and found the linear relationship between the friction coefficient and slope gradient rms value, and then he proposed an expression of the mean friction angle denoted by 3D morphology parameters. Kulatilake et al. (1995) applied the fractal method to study the roughness of joint surfaces and proposed a shear strength formula that could reflect the anisotropism of shear properties. According to the results from more than 50 direct shear tests under constant normal load (*CNL*), Grasselli (2006), Grasselli and Egger (2003) and Grasselli et al. (2002) proposed a shear strength formula containing 3D morphology parameters (A_0, θ^*_{max} and C) for a rock joint surface, in which A_0 is the maximum possible contact area for the specified shear direction, θ^*_{max} is the maximum apparent dip angle in the shear direction, and C is the roughness parameter. Xia et al. (2013) selected θ_{3s}, R_s and A_0 to describe 3D rock joint surface roughness and proposed a shear strength formula according to the relationship between the peak dilatancy angle and the foregoing 3D roughness parameters (θ_{3s}, R_s and A_0) based on Patton's formula, in which θ_{3s} is mean value of dip angle of area element facing to shear direction, R_s is the ratio of the unfolded area of the joint surface to its projective area. Different from Grasselli (2001), A_0 is the maximum possible contact area ratio of total value of dip angle of area element facing to shear direction to the unfolded area of the joint surface. According to Maksimović's (1992) model for the angle of shearing resistance, there is a hyperbolic relationship between dilatancy angle and normal stress. Hence, Tang and Liu (2015) proposed a shear strength formula of a rock joint based on Maksimovic's model. Additionally, a number of shear strength formulas have been proposed by other authors (Amadei et al. 1998; Saeb and Amadei 1992; Plesha 1987; Seidel and Haberfield 2002; Johansson and Stille 2014; Xia et al. 2014).

Overall, some progresses have been achieved in the study of the influence of the 3D morphology of a rock joint surface on the peak shear strength. However, the study on different types of fractured specimens may have some significance for understanding the

influences of 3D morphology parameters on shear strength of rock fractures. Thus, the authors conducted direct shear tests on five groups of rock fractures (including sandstone, powder-grained marble, fine-grained marble, medium-grained marble and coarse-grained marble) under different *CNL* and measured the 3D morphology parameters of rock fracture surfaces with the goal of proposing a shear strength formula containing 3D morphology parameters.

2 Introduction of Direct Shear Test

2.1 Test Apparatus

The direct shear test system (RDS-200) designed by Geotechnical Consulting and Testing Systems (GCTS) is used in this research, as shown in Fig. 1. The system automatically controls shear and normal load by the electro-hydraulic servo system. The shear boxes consist of two circular platens, whose upper and lower platens are open at the center. The shear and normal load capacities of this shear system are 10 t and 5 t, whereas the shear and normal strokes are 25 and 24 mm, respectively.

3D morphologies of the rock fracture surfaces are obtained using the 3D scanner designed by TenYoun 3D Technology Corporation and Tsinghua University, as shown in Fig. 2 (left). The 3D scanning model is shown in Fig. 2 (right). The global error control module is included to control the scanning accuracy of the surface morphology. The average accuracy is 0.02–0.03 mm. The scanner can cover a maximum scanning area of 400 × 300 mm^2.

2.2 Specimen Preparation

First, cylindrical specimens with a diameter and length of approximately 50 and 100 mm were prepared from the rock block. Second, tensile fractures were produced at or near the mid-height of the specimen by self-made split tool as shown in Fig. 3 (left). The self-made split tool including two parts has a cylinder surface whose radius is almost equal to the specimen. Each part has a cylindrical groove which is embedded with a wedge-shape steel wire. Thus, uniform linear compression stress can be applied on the side surface of the specimen perpendicular to axis (Wang et al. 2016). According to the rock type and grain size, these specimens were divided into five groups, named S (sandstone), A (powder-grained marble), B (fine-grained marble), C (medium-grained marble) and D (coarse-grained marble), and each group was consisted of six specimens (Fig. 3 medium). Their physical and mechanical properties are shown in Table 1. In Table 1, φ_b was obtained through tilt test

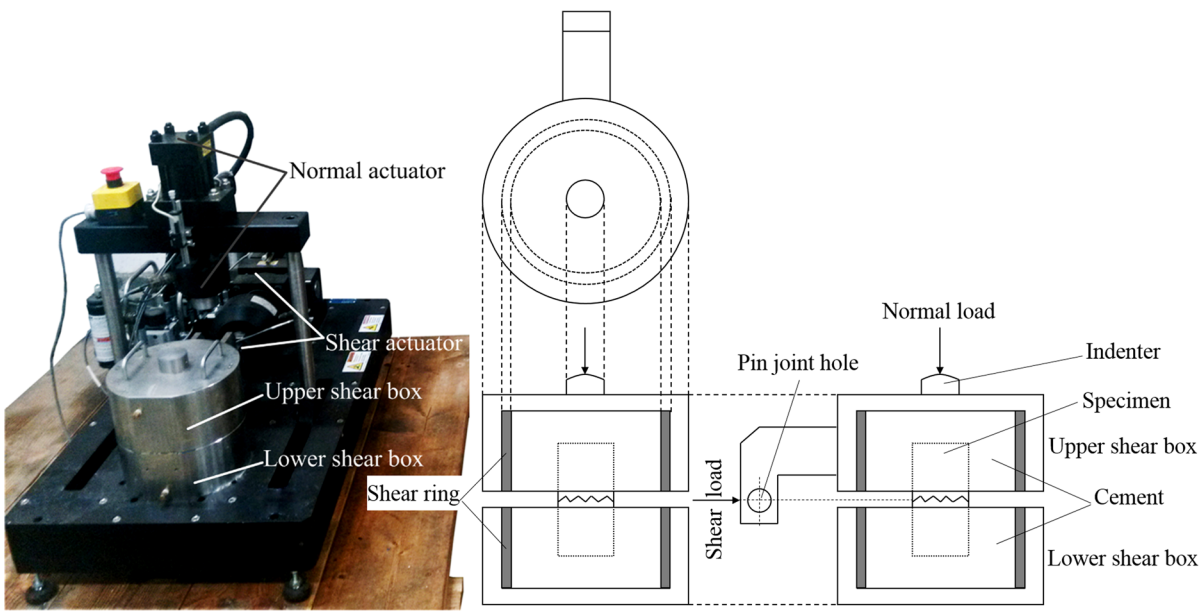

Fig. 1 RDS-200 direct shear testing system (*left*), cross-section of shear box (*right*)

Fig. 2 OKIO 3D scanner (*left*), 3D view of the fracture surfaces (*right*)

on flat dry unweathered rock surface. c_1 (Cohesion of rock fracture) and c_2 (Cohesion of rock specimens) were obtained through direct shear tests on rock fractures and triaxial compression tests on standard cylindrical rock specimens respectively. φ (Internal friction angle of rock specimens) was obtained from triaxial compression tests on standard cylindrical rock specimens. σ_t (Tensile strength of rock specimens) was obtained from brazilian split tests. E (Elastic modulus of rock specimens) and μ (Poisson's ratio of rock specimens) were obtained from uniaxial compression tests.

Before the test, fracture surfaces of all specimens were scanned to get their morphology data. Then the specimen was placed and fixed in the center hole of the lower and the upper shear ring by quick-setting cement according to the same method as reference (Li et al. 2015) (Fig. 3, right). Because this type of special fast-setting cement had a *UCS* of 80 MPa and Young's modulus of 30 GPa, the influence of the deformation of encapsulating material was so slight (less than 1% in this paper) that it could be ignored. The lower box is fixed while a horizontal force induced by the movement of the shear arm is applied to the upper box in the direction parallel to the fracture surface between the upper and lower boxes. Before the application of the horizontal force, a normal force was applied on the upper box perpendicular to the fracture surface by the

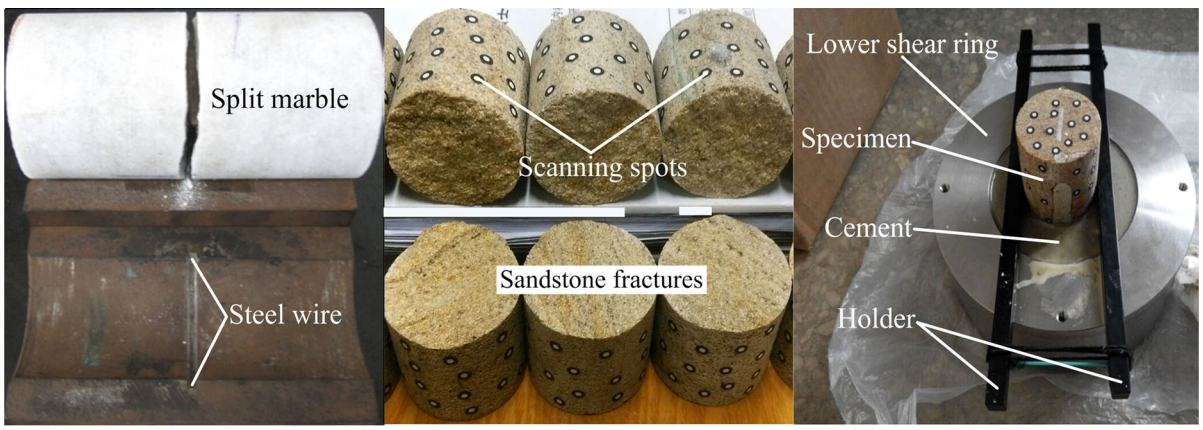

Fig. 3 Split tool (*left*), tensile fractures (*medium*), encapsulation of specimen (*right*)

Table 1 Mechanical properties of rock fractures and intact rock specimens

Specimen	φ_b (°)	*JCS* (MPa)	c_1 (MPa)	c_2 (MPa)	φ (°)	σ_t (MPa)	E (GPa)	μ
S	30.00	78.43	0.78	21.452	46.0	3.76	24.58	–
A	31.04	141.68	1.95	50.903	25.8	15.14	83.87	0.38
B	35.81	70.93	3.00	25.794	25.8	17.30	47.45	0.29
C	36.01	65.17	1.80	28.961	23.6	12.91	47.78	0.29
D	36.88	48.38	2.76	15.039	30.0	10.30	41.88	0.18

movement of the normal arm. To ensure the verticality of the normal load, the hydraulic jack applying the normal force is mounted to a frame that is able to travel with the upper box when the upper box is moved by a horizontal force. The apparatus is controlled by computer-aided testing software (CATS), and the test data can be imported into Excel or another software program when the test is complete.

2.3 Test Method

During the direct shear test, the specimens were sheared under a constant normal load (*CNL*) condition. Six levels of constant normal loads including 5, 10, 15, 20, 25 and 30 kN were applied to the fractured specimens. In addition, shear displacement control mode with a constant shearing rate of 1 mm/min was used to control the shear load. The shear displacements were set as approximately 5 mm for sandstone fractures and 10 mm for marble fractures. It is suggested that the shear displacement should be smaller than 5 mm for 50 mm diameter specimen in this paper. The constant normal loads from small to large (5–30 kN) were applied to each specimen in groups of S1–S6, A1–A6, B1–B6, C1–C6 and D1–D6. Because the contact area changes along with the shear displacement, the normal stress also changes under the constant normal load. Peak normal stress (σ_p) is the normal stress when peak shear stress happens, as shown in Table 2. In Table 2, *CNL* is constant normal load; i_a is average climbing angle at zero normal stress; i_{pm} is modified i_p (Predicted peak dilatancy angle); R_s is ratio of unfolded area to projective area for rock fracture surface; S_{dq} is 3D root mean square kurtosis; S_a is arithmetical mean deviation; S_q is root mean square deviation of the profile.

3 Shear Test Results Analysis

Figure 4 shows the complete shear stress-shear displacement curves of the 30 test specimens and the schematic diagram of typical curve of shear stress versus shear displacement. For most of the curves, the shear stresses under the *CNL* condition increase linearly to the peak point and then decrease sharply or gradually to residual values that remain within some stress intervals which are in agreement with the reference (Lee et al. 2014; Barton et al. 1985; Bandis et al. 1983). Figure 4 indicates that the peak shear strength generally appeared before the shear displacement reached 2.82 mm.

These shear stress-shear displacement curves can probably be divided into five phases, as shown in Fig. 4f: (1) Compaction phase (o–a), in which it is slightly convex upwards, corresponding to a closure of the joints (Grasselli 2001); (2) Elasticity phase (a–c), a nearly linear portion, corresponding to the elastic deformation of the fractures subjected to compression and shear loads; (3) Yield phase (c, d), in which it is concave downwards, corresponding to the progression of micro-cracks of asperities until the failure; (4) Softening phase (d, e), the curves drop sharply or gradually during this phase according to the normal stress level and the roughness of rock fracture surfaces; (5) Residual phase (e-) corresponding to the residual friction of the fractures, which is nearly horizontal.

The values of peak shear strength (τ_p), peak shear displacement (δ_p), peak dilatancy angle (i_c), residual friction coefficient (f_r), pre-peak shear stiffness (k_{sp}) and post-peak drop gradient(k_{sa}) can be obtained from Fig. 4a–e, and the relationships between above parameters and peak normal stress are shown in Fig. 5a–f.

From Fig. 5a, b we can see that there is a highly positive linear relationship between peak shear strength (τ_p), peak shear displacement (δ_p) and peak normal stress (σ_p) respectively. It can be also seen from Fig. 5b that the mean value of peak shear displacement δ_p varies from approximately 0.67–2.82 mm.

On the aspect of peak shear displacement, Barton (1982) considered that *JRC* was the major factor that influenced the peak shear displacement (δ_p) and proposed a formula to estimate δ_p. Wibowo (1994) considered that normal stress (σ_n) was the major factor that influenced the peak shear displacement (δ_p). Asadollahi (2009) considered that both *JRC* and normal stress (σ_n) influenced the peak shear displacement (δ_p), and there was a positive linear relationship between peak shear displacement (δ_p) and normal stress (σ_n), while a negative relationship between peak shear displacement (δ_p) and *JRC* value. In this study, there exists a highly positive linear relationship between peak shear displacement (δ_p) and peak normal stress (σ_p). It is worth mentioning that the shear displacement during shear test consists of mainly fracture deformation because the fast-setting

Table 2 Test conditions and 3D morphology parameters of specimens

Specimen	φ_b (°)
S	30.00
A	31.04
B	35.81
C	36.01
D	36.88

Specimen		*CNL* (kN)	σ_p (MPa)	i_a (°)	i_{pm} (°)	Z_2	R_s	S_{dq}	S_a	S_q
A	A1	5	2.576	15.187	14.214	0.211	1.036	0.560	0.481	0.696
	A2	10	5.228	13.475	12.232	0.178	1.028	0.376	0.210	0.295
	A3	15	7.793	12.684	11.374	0.167	1.025	0.420	0.237	0.338
	A4	20	10.453	13.739	12.070	0.179	1.029	0.557	0.346	0.462
	A5	25	13.056	15.082	13.273	0.213	1.036	0.641	0.386	0.574
	A6	30	15.757	15.007	12.978	0.221	1.035	0.814	0.579	0.812
B	B1	5	2.577	23.518	18.265	0.344	1.091	1.091	0.702	0.937
	B2	10	5.198	22.894	15.938	0.299	1.086	1.086	0.422	0.586
	B3	15	7.815	21.839	14.104	0.305	1.077	1.077	0.384	0.553
	B4	20	10.465	22.385	13.704	0.286	1.081	1.081	0.510	0.693
	B5	25	13.123	23.756	14.019	0.359	1.093	1.093	0.641	0.890
	B6	30	15.824	21.238	12.087	0.259	1.073	1.070	0.604	0.882
C	C1	5	2.580	22.155	17.640	0.314	1.080	0.872	0.413	0.664
	C2	10	5.175	24.085	17.325	0.336	1.095	0.737	0.441	0.627
	C3	15	7.816	21.935	14.821	0.279	1.078	1.157	0.650	0.940
	C4	20	10.429	23.442	15.123	0.326	1.090	0.922	0.610	0.815
	C5	25	13.173	21.124	13.104	0.282	1.072	0.955	0.639	0.875
	C6	30	15.877	19.630	11.830	0.279	1.062	0.590	0.376	0.538
D	D1	5	2.578	27.333	16.019	0.377	1.126	1.562	0.881	1.228
	D2	10	5.166	26.098	12.180	0.345	1.114	1.151	0.712	0.963
	D3	15	7.804	25.557	10.231	0.367	1.108	0.874	0.512	0.72
	D4	20	10.537	29.359	10.500	0.421	1.147	1.875	0.638	0.913
	D5	25	13.126	27.861	9.158	0.42	1.131	1.659	0.893	1.217
	D6	30	15.750	26.421	8.100	0.404	1.117	3.193	1.083	1.498
S	S1	5	2.678	19.713	17.262	0.351	1.062	0.75	0.381	0.563
	S2	10	5.395	20.260	16.834	0.264	1.066	0.682	0.355	0.500
	S3	15	8.111	23.669	18.994	0.334	1.092	0.695	0.349	0.486
	S4	20	10.806	21.974	17.133	0.288	1.078	0.783	0.518	0.730
	S5	25	13.649	22.777	17.461	0.311	1.085	0.814	0.381	0.545
	S6	30	16.437	23.634	17.802	0.418	1.092	0.743	0.383	0.518

cement here have a *UCS* of 80 MPa and Young's modulus of 30 GPa and the influence of the deformation of encapsulating material is slight and could be ignored.

From Fig. 5c, d we can see that there is a good inverse proportional connection between peak dilatancy angle (i_c), residual friction coefficient (f_r) and peak normal strength (σ_p) respectively, which means the shear failure of a rock fracture results in the reduction of fracture surface roughness. With increasing normal stress, the failure mode of the fracture surface and asperities experience a transition from slid-type to cut-type, and asperities rupture near their base under a relatively higher normal loading condition (Wang et al. 2015). The higher the normal load is, the smoother the fracture surfaces tend to be and thus the smaller the residual friction coefficient (f_r) tends to be.

The slope of the line tangent to the pre-peak shear stress–shear displacement curve at the point of 50% of the peak shear strength has been used here to determine pre-peak shear stiffness (k_{sp}) (Goodman 1974). Figure 5e shows that there is a lowly positive linear relationship between pre-peak shear stiffness (k_{sp}) and peak normal stress (σ_p). According to Li et al. (2008), for the tooth-shaped asperity fracture, the pre-peak shear stiffness (k_{sp}) of the rock fracture linearly increased with increasing normal stress. However,

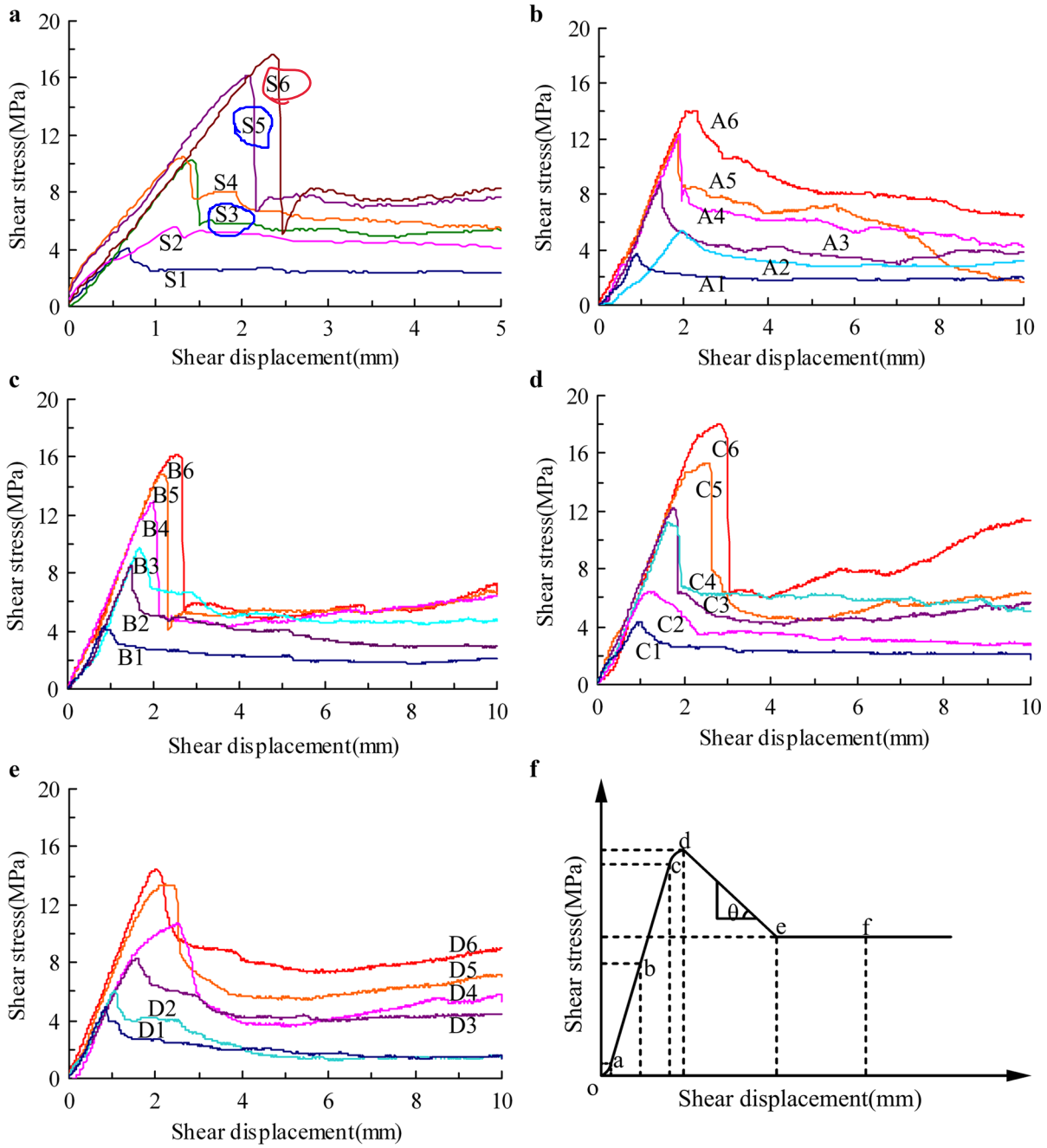

Fig. 4 Shear stress-shear displacement curves of the direct shear tests. **a** Sandstone, **b** powder-grained marble, **c** fine-grained marble, **d** medium-grained marble, **e** coarse-grained marble, **f** Schematic diagram of typical curve of shear stress versus shear displacement

Fig. 5e shows that the linear relationship between pre-peak shear stiffness (k_{sp}) and peak normal stress (σ_p) is not so obvious, which means that the pre-peak shear stiffness (k_{sp}) of the rock fracture may also have a connection with the rock fracture surface roughness. The increased fracture roughness would lead to increasing peak shear strength (τ_p) and pre-peak shear stiffness (k_{sp}) as presented in other references (Barton and Choubey 1977; Shang and Wei 2013).

During the direct shear test, a sharp decrease in shear stress is accompanied by a brief deep sound when shear failure occurred. To quantify the sharp

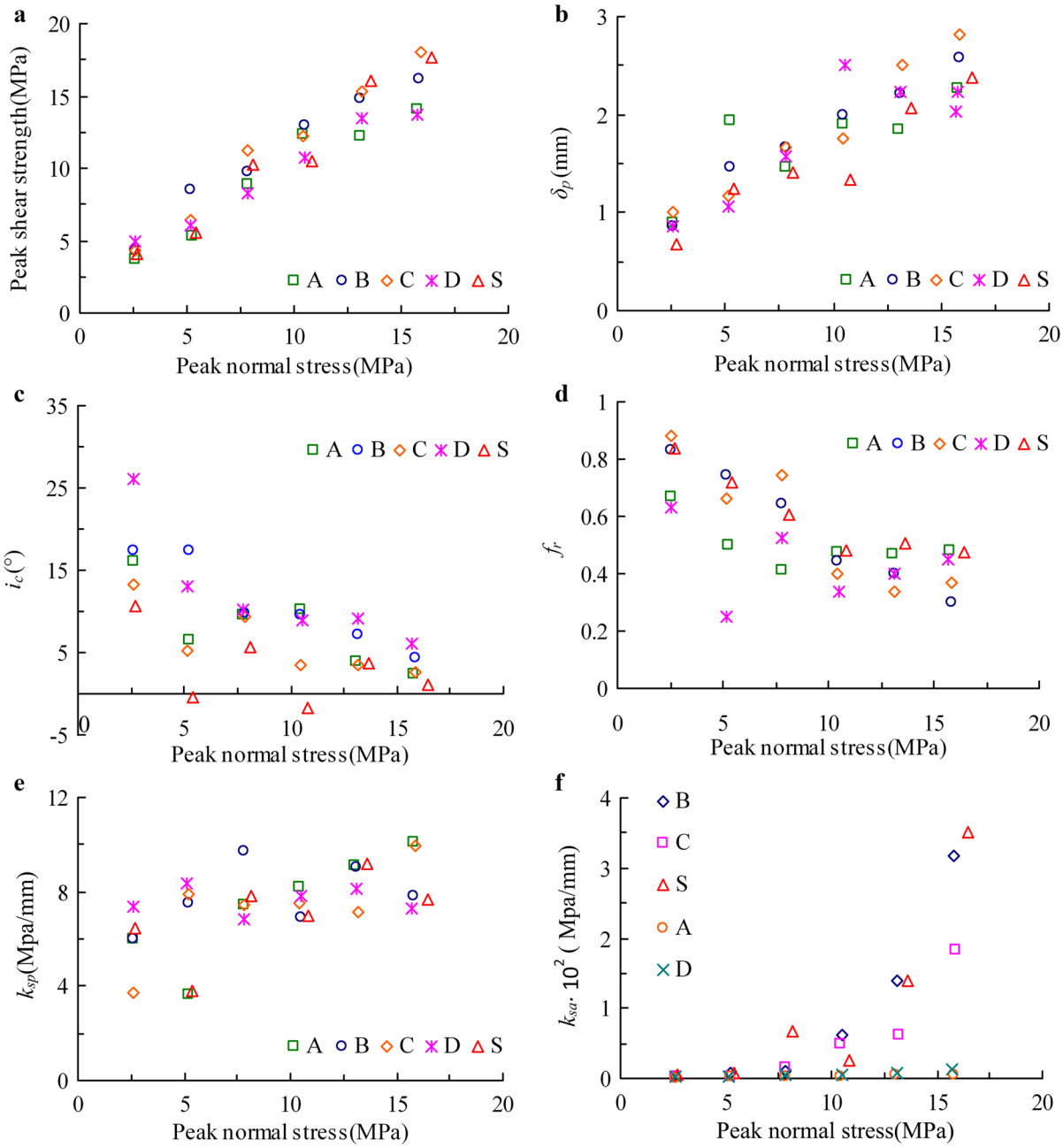

Fig. 5 **a** Peak shear strength versus peak normal stress, **b** peak shear displacement versus peak normal stress, **c** peak dilatancy angle versus peak normal stress, **d** residual friction coefficient versus peak normal stress, **e** pre-peak shear stiffness versus peak normal stress, **f** post-peak drop gradient versus peak normal stress

decrease in shear stress, the expression of the drop gradient (k_{sa}), which can be expressed as –tanθ, is proposed in this paper, as shown in Fig. 4f. The relationship between the drop gradient (k_{sa}) and the normal stress is obtained by fitting analysis as shown in Fig. 5f. Figure 5f shows that the drop gradient (k_{sa}) of each group of rock fractures exponentially increase with increasing normal stress, and their correlation coefficients are all greater than 0.87, as shown in Table 3. In Table 3, k_{sa} (MPa/mm) is drop gradient

after peak shear stress; σ_p (MPa) is peak normal stress. The higher normal load is, the bigger elastic strain of the asperities will experience. Thus, the big elastic energy accumulated under high normal stress and shear stress may sudden release and caused shear stress drop after peak.

4 New Shear Strength Formula of Rock Fracture

4.1 Modified Barton Formula

The *JRC* values could obtained either from tilt or pull tests on mated rough surface, or by visually comparing a rough fracture profile with the standard set of comparator profiles published by Barton and Choubey (1977). At present, *JRC* values might be also obtained by digitizing topography data of rock fracture surface with help of 3D scanning apparatus, and correlating roughness parameters with the published *JRC* values obtained by existing methods.

Relationships between *JRC* values and roughness parameters (Z_2, R_p, R_a, R_z, SF, M_s, λ, σ) had been proposed by many researchers and summarized in the latest articles (Li and Zhang 2015; Zheng and Qi 2016). Among them, Root mean square (Z_2) has the highest correlation coefficient (R^2) with *JRC* values as shown in Formula (4).

$$JRC_{2D} = 32.69 + 32.98\log_{10}(Z_2) \tag{4}$$

where JRC_{2D} is a two-dimensional (2D) fracture roughness coefficient. In this paper, the Z_2 values of four profile lines (1, 2, 3, 4), which mutually form an angle of 45 degrees between each two adjacent lines, are measured to obtain their average value with sampling interval of 0.5 mm, as shown in Table 2 and Fig. 6.

As for scale effects, Bandis et al. (1981) experimentally studied the scale effects on shear behavior of rock fractures. And then Barton and Bandis (1982) proposed the scale effect formulas about shear displacement, shear stiffness, *JRC* and *JCS*. Considering the scale effect of the rock fracture of *JRC*, the modified JRC_{2D} can be expressed as (Bandis et al. 1981)

$$JRC_{2DM} = JRC_{2D}\left(\frac{L}{L_0}\right)^{-0.02JRC_{2D}} \tag{5}$$

where JRC_{2DM} is the modified JRC_{2D}, L is the diameter of the rock fracture surface, and L_0 is the initial diameter of the rock fracture (100 mm). By substituting Eq. (5) into the Barton formula (2), the modified Barton formula (6a) is obtained.

$$\tau_p = \sigma_p \tan\left\{\varphi_b + JRC_{2DM}\log_{10}\left(\frac{JCS}{\sigma_p}\right)\right\} \tag{6a}$$

The calculated values of the modified Barton formula (6a) are obtained and compared with the experimental values of the peak shear strength of the rock fractures as shown in Fig. 7a. According to Fig. 7a, we can find that the predicted values of shear strength by modified Barton formula (6a) are acceptable in comparison with experimental values except that predicted peak shear strength values of D group are bigger than their experimental values. It may because the D group has lower *JCS* values as shown in Tab 1 (average *JCS* value of 48.38 MPa).

But Johansson (2015) suggested that no scale effect may exist for unweathered and perfectly mated rock fractures. By substituting Eq. (4) into the Barton

Table 3 Fitting equations of k_{sa} and σ_p

Specimen	Fitting equations	R^2
A	$k_{sa} = 0.82e^{0.12\sigma p}$	0.9146
B	$k_{sa} = 1.06e^{0.36\sigma p}$	0.9783
C	$k_{sa} = 0.72e^{0.36\sigma p}$	0.9614
D	$k_{sa} = 2.22e^{0.10\sigma p}$	0.9507
S	$k_{sa} = 2.36e^{0.30\sigma p}$	0.8703

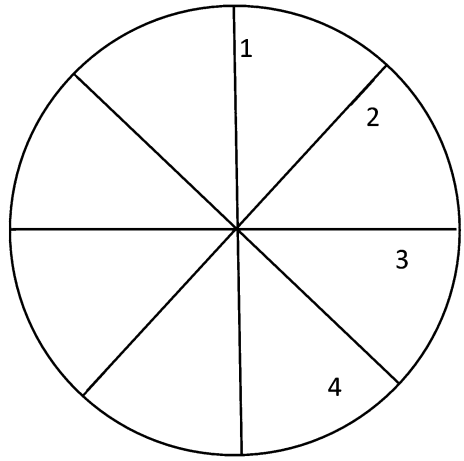

Fig. 6 Sketch map of profile lines

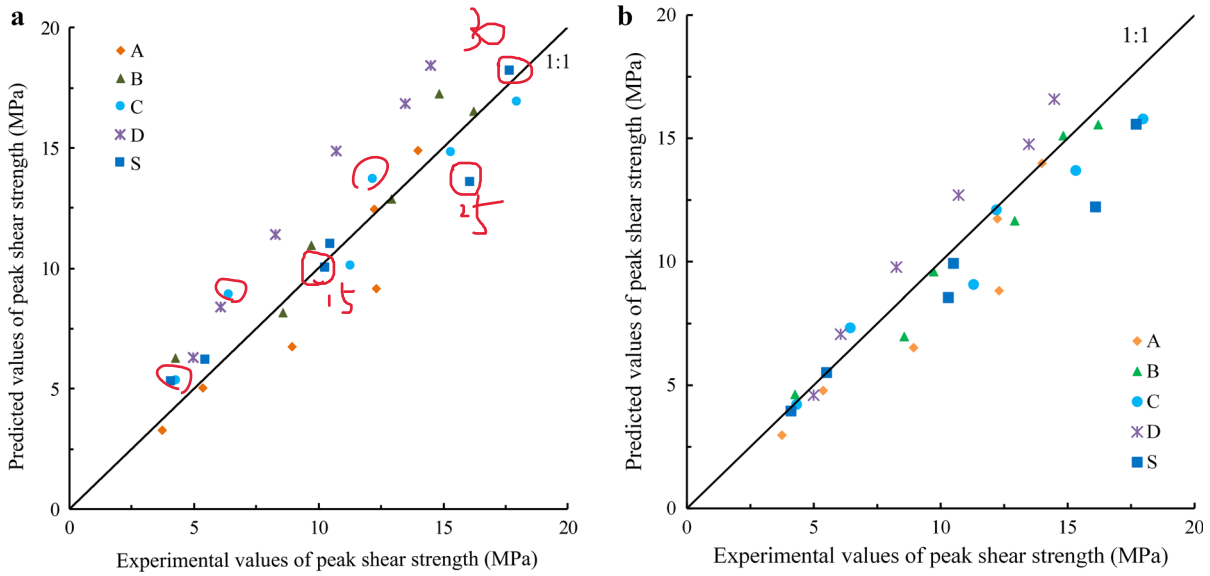

Fig. 7 **a** The comparison of peak shear strength between predicted values of modified Barton formula (6a) and the experimental values (**b**) The comparison of peak shear strength between predicted values of modified Barton formula (6b) and the experimental values

formula (2) directly, the modified Barton formula (6b) without considering scale effect is obtained.

$$\tau_p = \sigma_p \tan\left\{\varphi_b + JRC_{2D}\log_{10}\left(\frac{JCS}{\sigma_p}\right)\right\} \tag{6b}$$

The calculated values of the modified Barton formula (6b) without considering scale effect are obtained and compared with the experimental values of the peak shear strength of the rock fractures as shown in Fig. 7b. Through the comparison between Fig. 7a, b, it is found that Formula (6b) (without considering scale effect) show a little better predicted results than Formula (6a) (considering scale effect). Especially predicted results of D group calculated by Formula (6b) are much closer to line y = x than Formula (6a). Moreover, the standard deviation of predicted values of Formula (6a) and Formula (6b) is 1.918 and 1.566 respectively. Thus, it is concluded that scale effect tend to be not obvious for unweathered and perfectly mated rock fractures whose diameter is 50 mm (smaller than 100 mm) in this paper.

4.2 New Shear Strength Formula

According to the projective theorem of an area, the projective area equals the product of the original area and the cosine value of the intersection angle, as shown in Fig. 8. R_s, which reflects the roughness of the fracture surface, equals the ratio of the unfolded area of the fracture surface to its projective area. If it is assumed that S_1 equals the unfolded rock fracture surface and S_2 equals the projective area of the rock fracture surface, the dihedral angle could be regarded as the average climbing angle i_a of the rock fracture surface. Thus, the calculation formula of i_a is developed as follows, and the values of i_a are listed in Table 2.

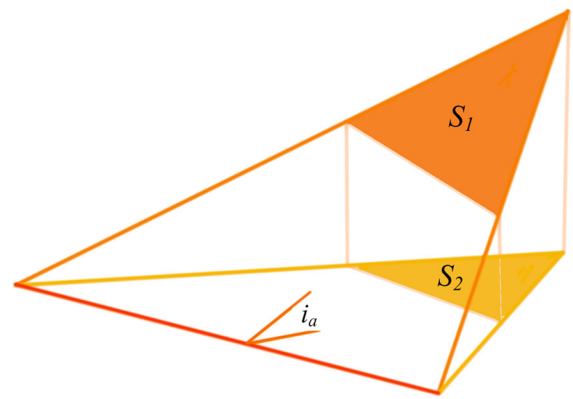

Fig. 8 The dihedral angle between projection and original plane

$$i_a = \arccos(1/R_s) \tag{7}$$

There exist two kinds of failure modes in this research which are sliding mode and cutting mode of

asperities respectively (Patton 1966). By substituting Formula (7) into (1), we obtain the sliding mode

$$\tau_p = \sigma_p \tan[\varphi_b + \arccos(1/R_s)] \tag{8}$$

Patton (1966) considered that changes in the slope of a failure envelope reflected changes in the failure modes, and changes in the failure modes were related to joint strength parameters and effective climbing angle. In this research, the rough value of critical normal stress was obtained by plotting and comparing the predicted shear strength values of Formula (8) with their experimental values, as shown in Fig. 9a. If the predicted shear strength by formula (8) is about equal to its corresponding experimental value, it could be regarded as sliding failure mode. Otherwise, it should be cutting failure mode. According to Fig. 9 (a), it is showed that failure in sliding mode happened under low normal stress; while failure in cutting mode happened under high normal stress. On the whole, high *JCS* of specimen leads to much higher critical normal stress as shown in Fig. 9b.

As for the cutting failure mode, according to the evolution trends of the peak dilatancy angle (i_c) along with the peak normal stress (σ_p) as shown in Fig. 5c, Formula (9) based on the 3D morphology parameter (R_s) and peak normal stress (σ_p) is proposed to estimate the predicted peak dilatancy angle i_p.

$$i_p = \frac{i_a}{\sigma_p + 1} \tag{9}$$

By substituting Formula (9) into (1), we obtain

$$\tau_p = \sigma_p \tan\left[\varphi_b + \frac{\arccos(1/R_s)}{\sigma_p + 1}\right] \tag{10}$$

The relationship between predicted values using Formula (10) and the experimental values is shown in

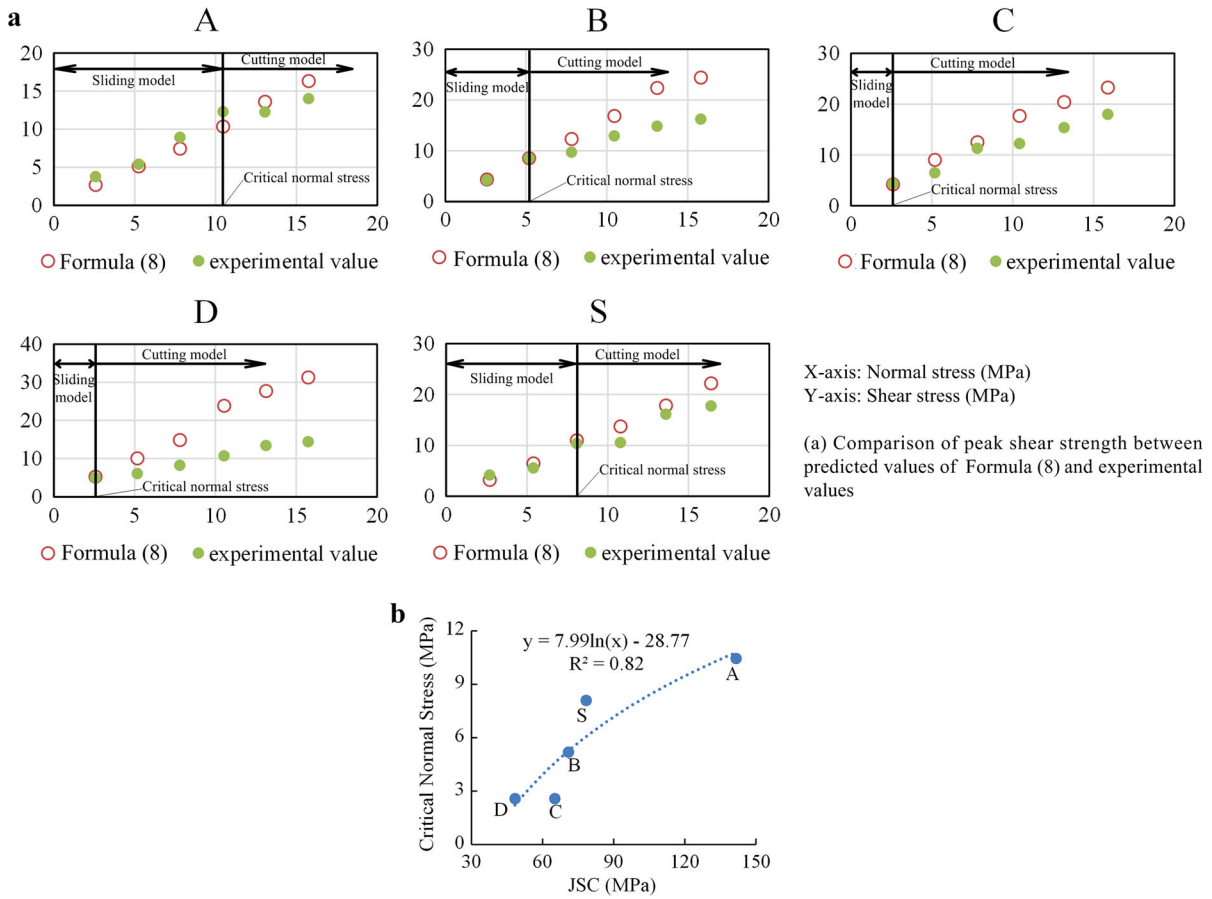

Fig. 9 **a** Comparison of peak shear strength between predicted values of Formula (8) and experimental values, **b** relationship between critical normal stress and *JCS*

Fig. 10. From Fig. 10 we can see that most predicted values of Formula (10) are smaller than their experimental values. The standard deviation of predicted values of Formula (10) is 4.084. The reason of less-than-ideal predicted values of the peak shear strength may be that this formula underestimates the influence of normal stress on shear strength of rock fracture. Therefore the correction coefficient (m) is induced to reflect the influence of normal stress on shear strength of rock fracture. Thus, the corrected i_{pm} is expressed as follows:

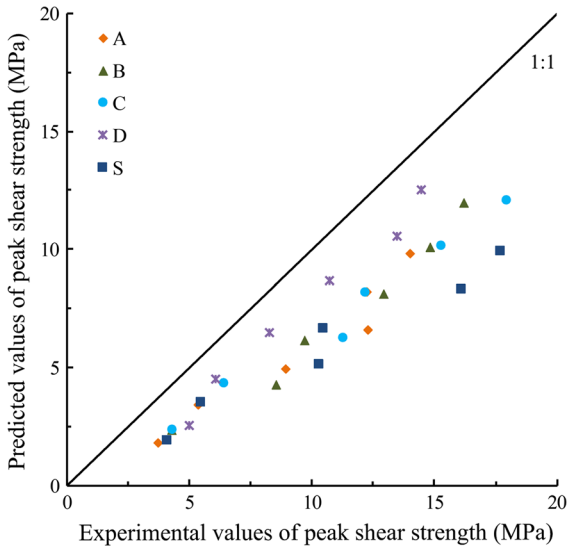

Fig. 10 The comparison of peak shear strength between predicted values of Formula (10) and the experimental values

$$i_{pm} = \frac{\arccos(1/R_s)}{(\sigma_p + 1)^m} \tag{11}$$

By substituting Formula (11) into (1), we obtain

$$\tau_p = \sigma_p \tan\left[\varphi_b + \frac{\arccos(1/R_s)}{(\sigma_p + 1)^m}\right] \tag{12}$$

When the fracture surface is flat, $i_a = 0$, and the proposed Formula (12) is reduced to $\tau_p = \sigma_p \tan\varphi_b$. m is obtained here when the predicted shear strength using Formula (12) is the nearest experimental values (based on the least square method). The relationships between correction coefficients (m) and average values of S_{dq}, S_a, S_q, UCS are shown in Fig. 11(a, b). S_{dq}, S_a, S_q and UCS have relatively close relationships with m, the correlation coefficients are all above 0.89. Thus, the fitting curves in Fig. 11 can be used to determine the correction coefficient (m) when we have the values of S_{dq}, S_a, S_q of different rock fractures or UCS of rock specimens. Finally, S_{dq} was used to determine correction coefficient (m) in this article based on its highest correlation coefficient.

The standard deviation of predicted values of Formula (12) is 1.085 which is smaller than Formula (6a, 6b and 8). The predicted values of peak shear strength by Formula (12) are shown in Fig. 12, where the predicted shear strength using Formula (12) has more close values with experimental results than that using Formula (6b) and Formula (10). Therefore, Formula (12) can be used to predict the peak shear

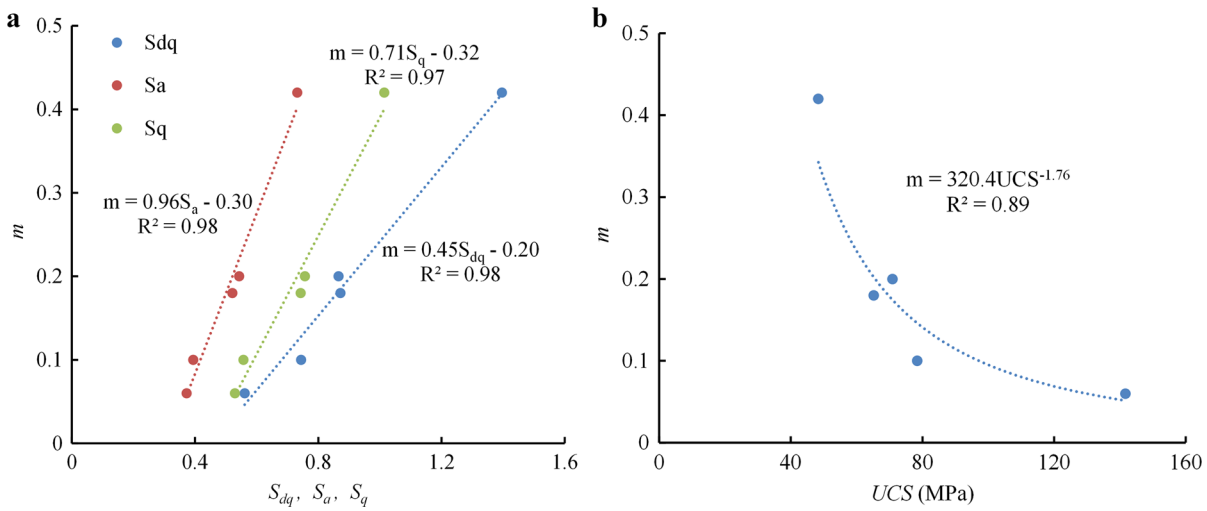

Fig. 11 **a** The relationship between correction coefficient (m) and average values of roughness parameters (S_{dq}, S_a, S_q); **b** the relationship between correction coefficient (m) and UCS

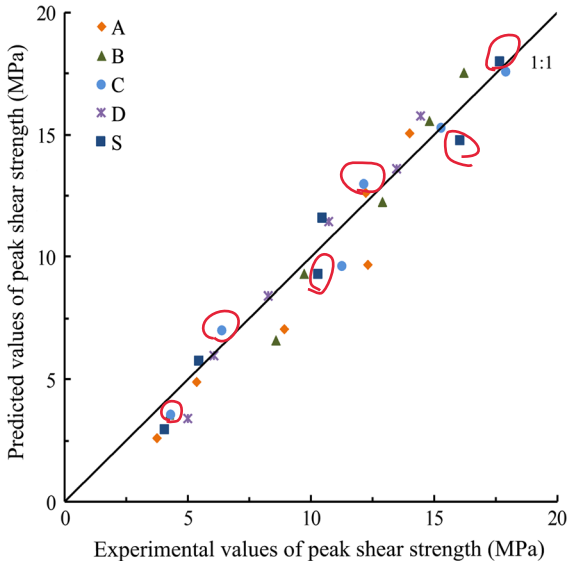

Fig. 12 The comparison of peak shear strength between predicted values of Formula (12) and the experimental values

strength (τ_p) of rock fractures and the parameters (φ_b, R_s, m) required in the formula can be obtained by conducting routine laboratory tests. Additionally, it is worth mentioning that Formula (12) can be used for both sliding failure mode and cutting failure mode of rock fracture from above results. Because when *UCS* of rock specimen is large, rock fracture surface is smooth or the normal stress is lower, Formula (12) could degenerate to Formula (8).

5 Discussions

Formula (8) can be used to describe the shear strength of rock fracture in sliding failure mode when normal stress is low enough, and in this condition, original morphology of rock fracture surface could be used to predict the shear strength of rock fracture. Essentially, just like Formula (8), Formula (12) is also used to describe sliding failure mode of rock fracture, but it considers the change of morphology of fracture surface caused by normal stress and original morphology. When normal stress is low, the climbing angle in Formula (8) is determined only by morphology parameter R_s which determines the shear resistance of rock fracture in only sliding failure mode, and now the morphology of fracture surface without break of asperities needn't to be modified. As normal stress increases, cutting failure will occur in rock fracture asperities, thus the morphology of rock fracture surface will change. Formula (8) will be changed as Formula (12) to describe the changed real morphology of fracture surface here, so that Formula (12) doesn't include Cohesion c_1. The reasons that correction coefficient m is induced in Formula (12) are as follows: normal stress will indiscriminately modify the morphology of fracture surface because Formula (10) doesn't include correction coefficient m, which will lead to an obvious error. So that correction coefficient m that can reflect morphology of fracture surface and *UCS* of specimen should be induced in Formula (12) to obtain the changed real morphology of fracture surface modified by normal stress according to their different fracture surface morphology and *UCS* of specimen, thus Formula (12) can be obtained to get better predicted shear strength of rock fracture.

Additionally, Patton (1966) proposed two formulas to describe the shear strength of the rock fracture in sliding failure mode and cutting failure mode. When normal stress was lower than critical normal stress, Formula (1) was used to obtain shear strength of rock fracture in sliding failure mode. Otherwise, when normal stress was bigger than critical normal stress, the following formula was used to describe shear strength of rock fracture in cutting failure mode:

$$\tau_p = c_1 + \sigma_n \tan \varphi_b \tag{13}$$

Actually, Formula (1) only expresses the shear resistance of the rock fracture when sliding failure occurs, while Formula (13) treats cutting failure of the rock fracture as intact-rock-like sample without considering the influence of the morphology on shear strength of the rock fracture. As a result, using above two formulas cannot describe the failure mode that including both sliding and cutting failure of rock fracture asperities. However, For Formula (12), when the normal stress is lower, the rock fracture surface is smooth or the *UCS* of the rock specimen is large, Formula (12) can degenerate to Formula (8) which can be used to predict the shear strength of rock fracture in mostly sliding failure mode. For a rock fracture that has certain *UCS* and surface morphology, the cutting failure will increase in fracture surface with increase of normal stress, and then a coupled condition including both sliding failure and cutting failure will appear, Formula (12) still can be used to describe this phenomenon in whole range of normal stress in tests. As the normal stress increases continually to be large

enough (but it cannot break the specimen), obvious shear dilatancy won't occur in rock fracture and the sliding failure will also reduce apparently. At this time, Formula (12) can still be applied to describe the shear strength of rock fracture in mostly cutting failure mode. From above analysis we can see that Formula (12) can describe more complex failure mode of rock fracture.

However, in the current research of this paper, no attempt is made to investigate the influence of rock fracture size or shear direction on peak shear strength, and further work is required to improve our full understanding of the shear failure mechanism of different types of rock fractures.

6 Conclusions

1. A typical curve of shear stress versus shear displacement is proposed based 30 shear stress–shear displacement curves and it can be divided into five phases including compaction phase, elasticity phase, yield phase, softening phase and residual phase.
2. The relationships between τ_p, δ_p, i_{pm}, k_{sp}, f_r, k_{sa} and σ_p are obtained respectively. In which peak shear strength (τ_p), peak shear displacement (δ_p) and pre-peak shear stiffness (k_{sp}) have linear relationships with peak normal stress (σ_p) respectively on the whole. And there is a good inverse proportional connection between peak dilatancy angle (i_c), residual friction coefficient (f_r) and peak normal stress (σ_p) respectively. Moreover, k_{sa} can express the sudden release of the elastic energy of the specimen and has a positively exponential relationship with σ_p.
3. On the aspect of shear strength formula of rock fracture, predicted values of shear strength by modified Barton formula (6b) with 2D morphology parameter show an acceptable result by comparing with experimental values. Thus, the modified Barton formula (6b) can be used to give reference and prediction of peak shear strength for mated rock fractures.
4. After determining the critical normal stress between sliding failure mode and cutting failure mode of rock fracture, a formula for predicting the shear strength of rock fracture in sliding failure is proposed based on a 3D morphology parameter R_s and another formula for both sliding and cutting failure mode of rock fracture is also proposed based on 3D morphology parameter R_s and S_{dq}. When UCS of specimens is large, rock fracture surface is smooth or the normal stresses are lower, the latter formula can degenerate to the former one, and it provides relatively accurate predicted shear strength of rock fracture through comparing of the predicted shear strength and the experimental values.

Acknowledgments This research is supported by the China National Natural Science Foundation (Project Nos. 51109076) and the key scientific and technological project of Henan Province (152102210316). The authors declare that they have no conflict of interest.

References

Amadei B, Wibowo J, Sture S, Price RH (1998) Applicability of existing models to predict the behaviour of replicas of natural fractures of welded tuff under different boundary conditions. Geotech Geol Eng 16(2):79–128

Asadollahi P (2009) Stability analysis of a single three dimensional rock block: effect of dilatancy and high-velocity water jet impact. Dissertation, University of Texas at Austin

Bandis S, Lumsden AC, Barton N (1981) Experimental studies of scale effects on the shear behavior rock joints. Int J Rock Mech Min 18:1–21

Bandis S, Lumsden AC, Barton N (1983) Fundamentals of rock joint deformation. Int J Rock Mech Min 20:249–268. doi:10.1016/0148-9062(83)90595-8

Barton N (1973) Review of a new shear-strength criterion for rock joints. Eng Geol 7(4):287–332. doi:10.1016/0013-7952(73)90013-6

Barton N (1982) Modelling rock joint behavior from in situ block tests: implications for nuclear waste repository design. Columbus: Office of Nuclear Waste Isolation

Barton N, Bandis S (1982) Effect of block size on the shear behavior of jointed rocks. In: Proceedings of the 23rd US symposium on rock mechanics, Berkeley, pp 25–27

Barton N, Bandis S (1990) Review of predictive capabilities of JRC-JCS model in engineering practice. In: Proceedings of international conference on rock joints, Rotterdam, Netherlands; pp 603–610

Barton N, Choubey V (1977) The shear strength of rock joints in theory and practice. Rock Mech Rock Eng 10(10):1–54. doi:10.1007/bf()1261801

Barton N, Bandis S, Bakhtar K (1985) Strength deformation and conductivity coupling of rock joints. Int J Rock Mech Min 22:121–140

Goodman RE (1974) The mechanical property of joints. In: Proceedings of the 3rd congress ISRM. Denver, pp 127–140

Grasselli G (2001) Shear strength of rock joints based on quantified surface description. Dissertation University of Parma

Grasselli G (2006) Manuel Rocha Medal Recipient Shear strength of rock joints based on quantified surface description. Rock Mech Rock Eng 39(4):295–314

Grasselli G, Egger P (2003) Constitutive law for the shear strength of rock joints based on three-dimensional surface parameters. Int J Rock Mech Min 40(1):25–40. doi:10.1016/S1365-1609(02)00101-6

Grasselli G, Wirth J, Egger P (2002) Quantitative three-dimensional description of a rough surface and parameter evolution with shearing. Int J Rock Mech Min 39:789–800

Jing L, Stephansson O, Nordlund E (1993) Study of rock joints under cyclic loading conditions. Rock Mech Rock Eng 26(3):215–232

Johansson F (2015) Influence of scale and matedness on the peak shear strength of fresh, unweathered rock joints. Int J Rock Mech Min 82:36–47

Johansson F, Stille H (2014) A conceptual model for the peak shear strength of fresh and unweathered rock joints. Int J Rock Mech Min 69:31–38. doi:10.1016/j.ijrmms.2014.03.005

Kulatilake PHSW, Shou G, Huang TH, Morgan RM (1995) New peak shear strength criteria for anisotropic rock joints. Int J Rock Mech Min 32(7):673–697. doi:10.1016/0148-9062(95)00022-9

Kusumi H, Teraoka K, Nishida K (1997) Study on new formulation of shear strength for irregular rock joint. Int J Rock Mech Min 34(s3–4):168.e1–168.e15. doi:10.1016/S1365-1609(97)00029-4

Ladanyi B, Archambault G (1970) Simulation of the shear behavior of a jointed rock mass. In: Proceedings of the 11th US symposium on rock mechanics. Berkeley, pp 105–125

Lee YH, Carr JR, Barr DJ, Haas CJ (1990) The fractal dimension as a measure of the roughness of rock discontinuity profiles. Int J Rock Mech Min 27(6):453–464

Lee YK, Park JW, Song JJ (2014) Model for the shear behavior of rock joints under CNL and CNS conditions. Int J Rock Mech Min 70:252–263. doi:10.1016/j.ijrmms.2014.05.005

Li Y, Zhang Y (2015) Quantitative estimation of joint roughness coefficient using statistical parameters. Int J Rock Mech Min 77:27–35

Li HB, Liu B, Feng HP, Zhang LQ (2008) Study of deformability behavior and failure mechanism by simulating rock joints sample under different loading conditions. Rock Soil Mech 29(7):1741–1752

Li WF, Bai JB, Chen JY, Peng Syd, Liu HL (2015) Determination of coal–rock interface strength by laboratory direct shear tests under constant normal load. Int J Rock Mech Min 77:60–67. doi:10.1016/j.ijrmms.2015.03.033

Maerz NH, Fanklin JA, Bennett CP (1990) Joint roughness measurement using shadow profilometry. Int J Rock Mech Min 27(5):329–343

Maksimović M (1992) New description of the shear strength for rock joints. Rock Mech Rock Eng 25(4):275–284

Patton FD (1966) Multiple modes of shear failure in rock. In: Proceedings of the first congress of international society of rock mechanics, Lisbon, pp 509–513

Plesha ME (1987) Constitutive models for rock discontinuities with dilatancy and surface degradation. Int J Numer Anal Methods Geomech 11(4):345–362

Reeves MJ (1985) Rock surface roughness and frictional strength. Int J Rock Mech Min 22(6):429–442

Saeb S, Amadei B (1992) Modelling rock joints under shear and normal loading. Int J Rock Mech Min 29(3):267–278. doi:10.1016/0148-9062(92)91657-Q

Sanei M, Faramarzi L, Goli S, Fahimifar A, Rahmati A, Mehinrad A (2015) Development of a new equation for joint roughness coefficient (JRC) with fractal dimension: a case study of Bakhtiary Dam site in Iran. Arab J Geosci 8:465–475

Seidel JP, Haberfield CM (2002) A theoretical model for rock joints subjected to constant normal stiffness direct shear. Int J Rock Mech Min 39(5):539–553. doi:10.1016/S1365-1609(02)00056-4

Serrano A, Olalla C, Galindo RA (2014) Micromechanical basis for shear strength of rock discontinuities. Int J Rock Mech Min 70:33–46. doi:10.1016/j.ijrmms.2014.02.021

Shang Z, Wei JH (2013) Impaction of structural plane roughness on deformation character and strength character. J Beihua Univ (Nat Sci) 14(6):744–748

Tang ZC, Liu QS (2015) Shear strength criterion and shear components of rock joints I: shear strength criterion. Chin J Geotech Eng 37(2):292–298

Tse R, Cruden DM (1979) Estimating joint roughness coefficient. Int J Rock Mech Min 16:303–307

Wang JA, Wang YX, Cao QJ, Ju Y, Mao LT (2015) Behavior of microcontacts in rock joints under direct shear creep loading. Int J Rock Mech Min 78:217–229. doi:10.1016/j.ijrmms.2015.05.002

Wang CL, Guo BH, Wang L (2016) Experimental study on relationship between mechanical, seepage characteristics and 3D morphology parameters of marble joint. Open Civil Eng J 10:513–523

Wibowo J (1994) Effect of boundary conditions and surface damage on the shear behavior of rock joints: tests and analytical predictions. Dissertation, University of Colorado

Xia CC, Tang ZC, Song YL (2013) A new peak shear strength formula for matching irregular joints based on 3D morphology parameters. Chin J Rock Mech Eng 32(supp. 1):2833–2839

Xia CC, Tang ZC, Xiao WM, Song YL (2014) New peak shear strength criterion of rock joints based on quantified surface description. Rock Mech Rock Eng 47(2):387–400

Xie HP, Wang JA, Kwasniewski MA (1999) Multifractal characterization of rock fracture surfaces. Int J Rock Mech Min 36:19–27

Zheng B, Qi S (2016) A new index to describe joint roughness coefficient (JRC) under cyclic shear. Eng Geol 212:72–85